View metadata, citation and similar papers at core.ac.uk

brought to you by CORE

provided by DigitalCommons@USU

Utah State University

DigitalCommons@USU

Conference Proceedings

Materials Physics

2018

Secondary Electron Yield Measurements of Carbon Nanotube Forests: Dependence on Morphology and Substrate

Brian Wood
Utah State University

Justin Christensen
Utah State University

Gregory Wilson
Utah State University

T. -C. Shen
Utah State University

JR Dennison
Utah State Univesity

Follow this and additional works at: https://digitalcommons.usu.edu/mp_conf

Recommended Citation

Wood, Brian; Christensen, Justin; Wilson, Gregory; Shen, T. -C.; and Dennison, JR, "Secondary Electron Yield Measurements of Carbon Nanotube Forests: Dependence on Morphology and Substrate" (2018). SCTC. *Conference Proceedings.* Paper 45.
https://digitalcommons.usu.edu/mp_conf/45

This Conference Paper is brought to you for free and open access by the Materials Physics at DigitalCommons@USU. It has been accepted for inclusion in Conference Proceedings by an authorized administrator of DigitalCommons@USU. For more information, please contact digitalcommons@usu.edu.

Secondary Electron Yield Measurements of Carbon Nanotube Forests: Dependence on Morphology and Substrate

Brian Wood, Justin Christensen, Greg Wilson, T.-C. Shen, J.R. Dennison

Abstract—**Total, secondary and backscatter electron yield data were taken with beam energies between 15 eV and 30 keV to determine the extent of suppression of substrate yields caused by carbon nanotube (CNT) forest coatings on substrates. CNT forests are low density graphitic carbon structures of vertically oriented CNT's. Chemical vapor deposition (CVD) was used to grow multi-walled CNT forests between 20-50 μm tall on a thick silicon substrate capped with a 3 nm diffusion barrier of evaporated aluminum. CNT forests can potentially lower substrate yield due to both its inherent low yield carbon composition and its bundled, high aspect ratio structure. In general, low-Z (atomic number) and low mass density conductors such as carbon have a lower density of bulk electrons for the incident electrons to interact with, thereby reducing secondary electron production. Rough surfaces, and in particular surfaces with deep high-aspect-ratio voids, can also suppress yields as electrons emitted from lower lying surfaces are recaptured by surface protrusions rather than escaping the near-surface region. Modification of yields from coatings can be modeled essentially serially, as layered materials with different yield curves. However, it is shown that suppression of yields due to CNT forest morphology is more significant than simple proportional contributions of components, and is related to the angular distribution of backscattered and secondary electrons as a function of energy. These two effects are expected to be most pronounced at low energies, where the incident electrons interact preferentially with the carbon at the surface.**

This study measured yields from three CNT forests of varied height and density, along with yields of an annealed substrate and constituent bulk materials. At incident electron energies above ~1200 eV the substrate yields dominated those of the CNT forests, as incident electrons penetrated through the low-density, low-Z CNT forests and backscattered from the higher-Z substrate. At lower energies <1200 eV, the CNT forests substantially reduced the overall yields of the substrate, and for <500 eV CNT forest yields were <1, well below the already low yields of bulk graphite. The yield's dependence on the height and density of the CNT forest is also discussed. By understanding these effects on electron yield, CNT growth can be catered for specific environments to mitigate spacecraft charging.

Index Terms—**Electron emission, carbon nanotube forests, chemical vapor deposition, secondary electron yield.**

I. Introduction

There is significant interest in reducing secondary electron emission from materials used for a variety of applications. This can be done by using bulk materials with intrinsically low electron yield, coating surfaces with low-yield materials [1-5], modifying the surface morphology [2,4-6], or with the use of nanocomposite material combining conducting and insulating particles to produce surface potential barriers that inhibit emission [7-9].

Selection of low-Z conductors limits the incident electron interaction with bulk electrons, thereby reducing the yields [1-5], and is typified by use of colloidal carbon coatings such as Aquadag™ to cover surfaces of electron optics elements and accelerator beam pipes.

Rough surfaces can also suppress yields, as electrons emitted from lower lying surfaces are recaptured by surface protrusions rather than escaping the near-surface region. The effect of surface roughness on electron yield has been extended to materials of high aspect ratio with deep voids; such an example are carbon velvets which tend to reduce the secondary yield of untreated planar carbon [4]. Voids in high aspect ratio materials are an extreme example of this roughness effect that act essentially as deep Faraday cups, which are very efficient at trapping electrons.

Multipacting issues in accelerators and waveguides, where oscillating electric fields create an avalanche effect with the electron cloud, have been mitigated with coatings, surface treatments, and use of structured nanocomposite materials [1,2,4,6,8]. Efficiency of traveling wave tubes (TWT) for space communicating amplifiers has also been increased with the use of textured carbon coated electrodes for the collectors [3,4,7-9].

Modifications of yield due to CNT forest morphology are related to the angular distribution of backscattered and secondary electrons as a function of energy [10]. Understanding the energy dependence of secondary yield may help separate the contributions to the yield suppression from CNT forests and other low-yield materials. CNT forest coatings might even be used to increase the effectiveness of electron collection sensors, acting essentially as nanoscale Faraday cups.

While attempts to measure the secondary yield of individual nanotubes have been made [5], the present study focuses on the CNT forest samples as a whole, to determine the relative effects

[1]B. Wood, G. Wilson, T-C. Shen, and JR Dennison are affiliated with the Physics Department, Utah State University, Logan, UT 84322 USA (e-mail: brian.wood314@gmail.com, jr.dennison@usu.edu)

J. Christensen was a graduate student at Utah State University, Logan, UT 84322 USA. He is now with Sandia National Labs, Albuquerque, NM 87185 USA

on the yield from the material composition and morphology. Forest density, height, and presence of defects are the main morphology factors that are expected to influence yield reduction of the sample. Forest density relates to the average packing density of the nanotubes which, along with CNT forest height, determines the density of bulk electrons (C atoms) the incident electrons interact with, and the range that the incident electrons will penetrate into the sample.

Section II describes the growth process of CNT forests and the parameters that can be modified to produce varying height and density in forests. Characterization of CNT forests is done primarily with scanning electron microscopy (SEM). Section III briefly reviews some of the relevant aspects of electron yield production and the mechanisms that influence yields. Section IV outlines the experimental methods used in this study, followed by the results and conclusions of the yield measurements presented in Section V and VI.

II. CNT Forest Growth and Characterization

CNT forest samples were made in the Utah State University Nanofabrication Lab using a non-plasma enhanced wet chemical vapor deposition method. Substrates of n-type silicon wafer were used with a 3 nm layer of evaporated aluminum to produce the proper in-diffusion rate of catalyst atoms. The wafer was then diced into 1 cm^2 pieces and loaded into a tube furnace at 700 ºC. A chemical precursor of xylene with a smaller molar concentration of ferrocene was injected into the furnace, dissociating into hydrocarbons and byproducts along with iron atoms from the ferrocene. Hydrogen and argon carrier gas flowing into the furnace at 50 sccm facilitated even distribution. Iron atoms coalesce within the substrate to form catalyst particles, allowing free carbons to dissolve into the hot Fe particles. Once saturated, rings of carbon precipitate out of the catalyst, giving a base to tip growth mechanism to produce the energetically favored tubular formation [11]. Continued precursor supply supports the vertical growth of the nanotubes. Duration of growth and precursor volume tend to determine the height of the forest, while the molar concentration of ferrocene in the precursor influences the density of the forest, with higher concentration producing denser forests, but with the possibility of more defects.

Scanning Electron Microscopy (SEM) is used to determine the height of the forest, along with its relative density and the presence of defects. Figures 1(a) and 1(b) visually illustrate the differences in density of the denser AlSi 129 sample (0.5% ferrocene concentration) compared to the AlSi 132 sample (0.2% ferrocene concentration). Continued growth produces inconsistent density along the height of the forest; these images are taken at the base of the forests, where the density is lowest.

TABLE I
CNT Forest Characteristics

Sample	Height (μm)	Ferrocene (%)	Surface Coverage	Surface Density (μg/cm^2)
AlSi 127	24-27	0.5	0.90	150
AlSi 129	42-51	0.5	0.91	280
AlSi 132	27-32	0.2	0.82	160

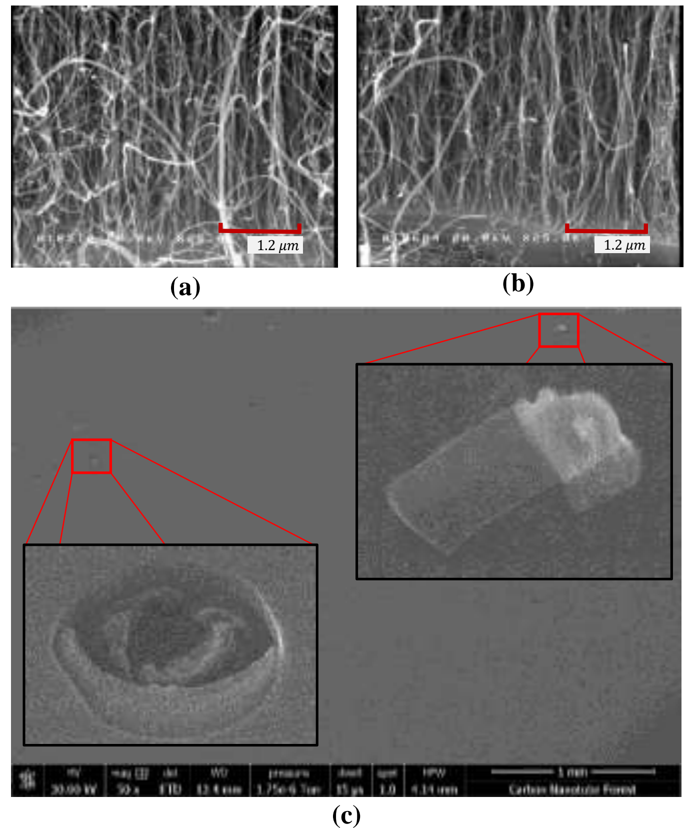

Fig. 1: Comparison of SEM images showing side-base views of the forest near the substrate interface for: (a) the denser AlSi-129 to (b) AlSi-132. (c) Top view of some typical surface defects of a sample, showing (left) deformations and (right) a substrate chip that gets dislodged and pushed to the top of the forest, with nanotubes growing off its edges

Defects are irregularities within or on the sample, including surface deformation from handling or dislodged catalyst and substrate particles. Figure 1(c) shows a typical surface deformation (bottom left), along with a substrate chip that has been pushed to the surface (top right), capable of growing nanotubes along its edges. The surface has the highest density and the most overturned CNT's, an effect more pronounced for samples of higher ferrocene concentration. Samples appear to have typical defects with no major deformations aside from AlSi 132, with portions of the sample having the forest actually scraped off, especially near the edges.

Table I lists sample heights, along with the molar ferrocene concentration during growth to distinguish the density differences. Surface coverage is also reported; this was found by counting the number of pixels above a threshold from top view photographs [12], although this is not fully indicative of bulk density within the forest. The bulk mass density of CNT forests grown by similar methods has been estimated as 0.02 g/cm^3 to 0.2 g/cm^3, or 1% to 10% of bulk graphite density of 2.2 g/cm^3. Densely packed vertically aligned nanotubes fabricated by a catalyst CVD method are reported to have mass densities on the order of 0.06 g/cm^3 [13]. While the wet-CVD method used for this study produces CNT's forests of less packing density, it does produce multi-walled CNT's of larger diameter, so it is reasonable to assume that the CNT densities are approximately the same. Surface density, as listed in Table

I, is calculated as 3% of the bulk graphite density times the surface coverage times the CNT forest height.

III. Electron Emission Theory

Electron yield is an incident energy-dependent measure of the interactions of incident electrons with a material and characterizes the number of electrons emitted per incident electron. The total electron yield (TEY), is defined as the ratio emitted electron flux to the incident flux,

$$\sigma(E) \equiv N_{out}^{e-} / N_{in}^{e-} \qquad (1)$$

Backscatter electron yield (BSEY) describes electrons emitted from the material which originate from the incident beam; operationally BSE are defined as electrons with emission energies >50 eV. Many BSE interact with the material largely through elastic (or nearly-elastic) collisions and are emitted with energies near the incident energy. Other BSE undergo one or many quasi-elastic collisions, but still escape with energies higher than most secondary electrons (SE). SE yield (SEY) describes electrons emitted from the material which originate within the material and are excited through inelastic collisions with the incident electrons; operationally SE are defined as electrons with emission energies <50 eV. SE emission spectra are typically peaked at 2-5 eV. SEY is determined by subtracting the BSEY from the TEY.

Figures (3) and (4) show secondary and backscattered electron yield curves. The SEY, δ, will typically rise above unity at energy E_1, reaching its maximum yield, δ_{max}, at a specific energy, E_{max}, and falling back below unity at energies above E_2. The energies E_1 and E_2 at which the yield crosses unity are called the crossover energies, where the number of emitted electrons is equal to the number of incident electrons and sample charging remains neutral. If the yield is below unity, a sample will charge negatively; if the yield >1, it is in a positive charging regime.

The interactions of electrons with the material depend on factors including the electron range, the stopping power of the material, and the energy barrier for escaping electrons to overcome; all these depend heavily on the incident electron. Once the electron passes into a material, the stopping power dictates how much energy is being deposited along its travel path; this deposited energy can lead to secondary electron generation, photon production (cathodoluminescence), enhanced conductivity (radiation induced conductivity), and phonon production among other effects [14]. The continuous slowdown approximation for the stopping power and range, states that the energy loss is a continuous (not discrete) function along its path through the material [15]. Once an incident electron has dissipated all of its energy, it will embed its charge in the material at a certain penetration depth. For SE and BSE to escape a material, the electron must have enough energy to cross the vacuum barrier, which is the work function for a conductor or the electron affinity for dielectrics and semiconductors [16]. Graphite being a semi-metal has a work function of 4.86 eV associated with it [17], and CNT have been shown to have similar work functions of ~5 eV [18].

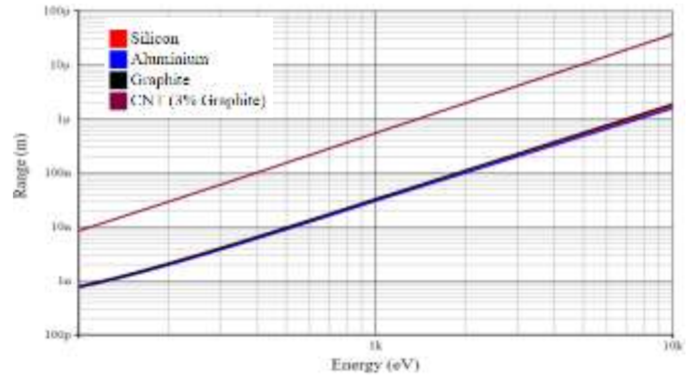

Fig. 2: Electron range versus incident energy for sample materials Al and Si (indistinguishable on this scale), bulk graphite (density of 2.2 g/cm^3), and graphite scaled to 3% of bulk graphite mass density.

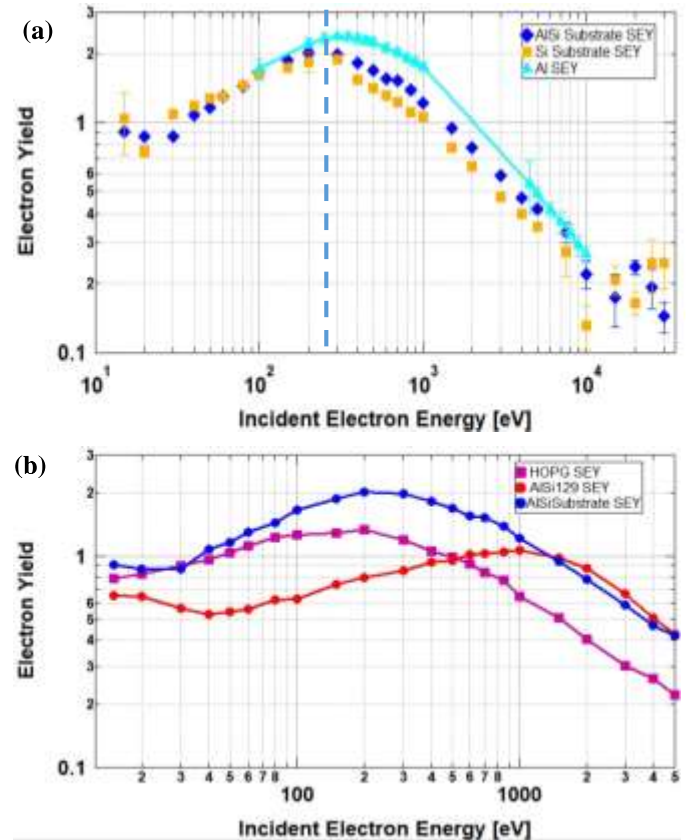

Fig. 3: Secondary electron yield measurements of component sample materials. (a) SEY versus incident energy of bulk Al and uncoated Si substrate, plus a bare coated AlSi substrate. The vertical dashed line indicates the energy of electrons with a 3 nm range. (b) SEY versus incident energy of bulk HOPG graphite [20], a bare coated AlSi substrate, and the AlSi 129 CNT forest sample.

Since a CNT forest is an inhomogeneous material, it has extreme asymmetries due to the high aspect ratio and hollow nature of the CNTs, and has many atomic and macroscopic defects, the transport and emission of electrons is not as straightforward. An electron can conduct preferentially along the length of the CNT, confining movement due to the orientation of the forest. Possibility of electron transfer from contacting tubes is conceivable, along with electrons emitting

from the side of a tube within the forest; these may result in additional energy loss mechanisms associated with transport within the CNT forest.

Analysis of multilayered and composite samples is facilitated by knowledge of the electron range (the maximum distance an incident electron of specific energy will penetrate into a material). Energy is lost at an approximately constant rate (constant loss approximation) as incident electrons traverse the material; hence, an approximately uniform distribution of internal secondary electrons with depth into the material is generated. Figure 2 shows the range versus incident energy calculated using a range tool developed by Wilson [19] for component materials bulk Al, Si, and bulk graphite (nearly indistinguishable on this scale), and graphite scaled to 3% of bulk graphite density (2.2 g/cm^3) as a surrogate for the low-density CNT forest samples.

IV. Experimental Setup

Electron yields were measured at the USU Space Environment Effects Materials (SEEM) test facility using a custom high vacuum (10^{-5} Pa) chamber [14,19,20]. Two monoenergetic pulsed electron gun sources were used, a lower energy (~10 eV - 5000 eV), low-current (<100 nA) gun (Staib Instruments Model EK-5-S) and a higher energy (5 keV - 30 keV), higher current (<10 μA) gun (Kimball, Model EGPS-21B). Pulses used were ~3-5 μs in duration at <1 nA-cm^{-2} beam current densities for small beam spots (1-2 mm diameter at 0.5 to 30 keV, increasing to ~7 mm diameter at 50 eV and lower). In general, energies below 30 eV may be less reliable as stray electric and magnetic fields and sample bias may alter low energy electron trajectories. Pulsed beams are implemented to reduce charging of insulators, along with a low energy ~5 eV flood gun and a ~5 eV UV LED used for a few seconds between each incident electron pulse to neutralize charge within insulating samples [11,21]. Energies above 5 keV have more variance in the pulses sent into the HGRFA, giving these measurements larger error.

Electron yields were measured using a fully-enclosed hemispherical grid retarding field analyzer (HGRFA) which determines absolute yield accurately (<5% absolute uncertainty) [11,21], since the encapsulating design captures almost all of the emitted electrons [11]. Concentric hemispherical grids are used both to energetically discriminate the collected electrons and to mitigate possible charging of the sample [15]. Electron pulses with varying energy impinge on the sample through the HGRFA via a drift tube. Currents traces are measured from the sample and five HGRFA detector elements, which are integrated over the pulse duration to determine the total charge associated with the individual currents. Biasing a retarding grid to 0 V and -50 V, respectively, allows determination of total and backscattered yield calculated via Eq. (1); the difference between total and backscattered yield is the secondary electron yield.

V. Results

We first consider the SEY of the Al coated Si substrate and its component materials to determine its influence on the CNT forest results. Comparison of SEY of bulk HOPG to the bare AlSi substrate, shows that carbon inherently has a lower SEY,

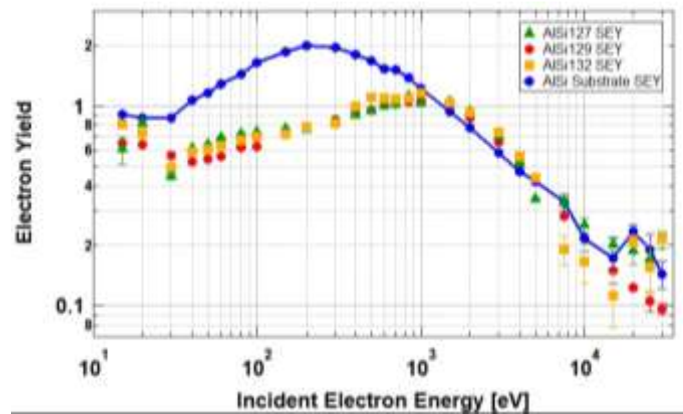

(a)

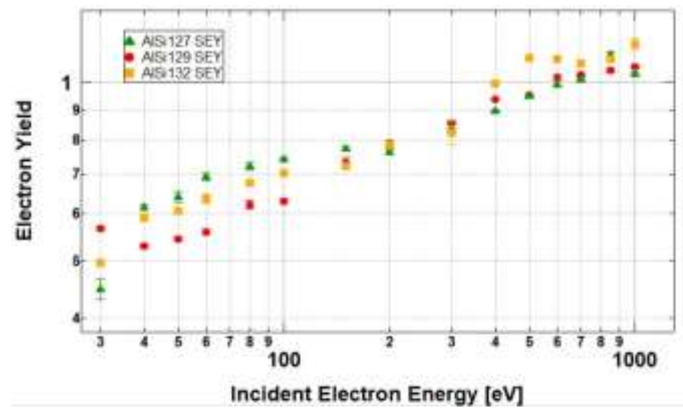

(b)

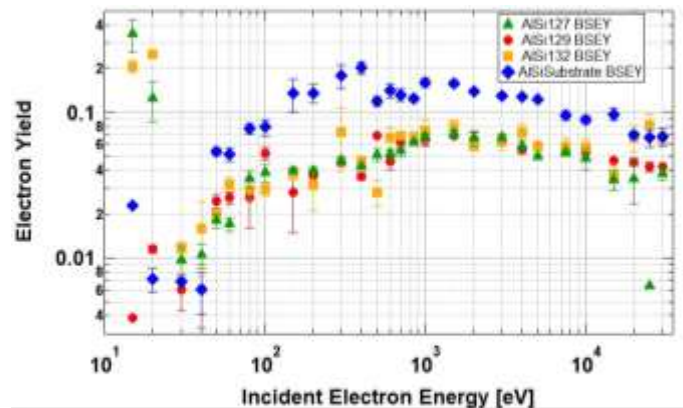

(c)

Fig. 4: Electron yield versus incident electron energy for AlSi 127, AlSi 129 and AlSi 132 CNT forest samples compared to a bare AlSi substrate SEY (a). (b) Showing variance in low energy SEY among the CNT forests samples. (c) BSEY of forest samples and AlSi substrate.

making it a good candidate material for electron suppression. Figure 3(a) shows the SEY of bulk Al, an uncoated Si substrate, and an Al coated Si substrate (designated AlSi). As expected, the yield curve for the coated AlSi sample is a direct combination of bulk Si and Al yield curves [21]. The SEY of the AlSi substrate is shifted to 8% higher E_{max} (see Table II) with a 7% increase in δ_{max}, as compared to the bare Si substrate. Below ~200 eV, the yield curves are indistinguishable, within measurement errors. Above ~200 eV, the yield of the coated AlSi substrate is consistently ~8% higher than pure Si up to 10 keV. Al has a ~29% higher δ_{max} and ~20% higher E_{max} than

TABLE II
Electron Yield Values.

	Secondary Yield				Backscattered Yield		
Sample	δ_{max}	E_{max} (eV)	E_1 (eV)	E_2 (eV)	η_0	η_{Peak}	E_{PEAK} (eV)
Si	1.88 ± 0.05	250	27	1080	0.08	0.17	1000
Al	2.35 ± 0.06	300	-	2040	0.18	0.27	350
Al on Si	2.02 ± 0.06	270	36	1375	0.09	0.17	1000
HOPG	1.34 ± 0.03	200	45	486	0.039	0.065	400
AlSi 127	1.11 ± 0.01	850	635	1680	0.039	0.065	1500
AlSi 129	1.06 ± 0.01	1000	568	1370	0.047	0.069	1800
AlSi 132	1.16 ± 0.02	1000	404	1650	0.06	0.07	1300

bulk Si. Together, the AlSi yield is higher than the bare Si substrate by ~30% of the difference between the bulk Al and Si yields. These increases are attributed to the 3 nm Al diffusion barrier, where a portion of the incident electrons start passing through the Al layer of the AlSi substrate at higher energies. From Fig. 2, the energy of a 270 eV electron is ~3 nm, so yield contributions from the AlSi substrate should be dominated by the Al coating below 200 to 300 eV, with the Al contribution falling off slightly faster than linearly at higher energies; the range increases with energy approximately as $E^{1.35}$ above E_{max} [22,23].

By contrast, the yield curves for the CNT forest samples are not a direct combination of the bare Al-coated Si substrate yield curve and a graphitic carbon yield curve, as is evident in Figs. 3(b) and 4(a). Fig. 3(b) shows SEY versus incident energy of bulk HOPG graphite [20], a CNT bare AlSi substrate, and the AlSi 129 CNT forest sample. Above ~1200 eV, the AlSi 129 yield curve is nearly identical to the AlSi substrate; that is, the effects of the CNT forest are minimal for energies where most energy is deposited in the AlSi substrate. From Fig. 2, the range in bulk graphitic carbon is ~50 nm at 1200 eV, or ~750 nm for the CNT surrogate with ~3% the density of bulk graphite. Alternately, the energy to penetrate ~35 μm of CNT with ~3% the density of bulk graphite is ~10 keV, a much higher energy than where the CNT forest sample yield curves begin to match the bare AlSi substrate yield curve. This suggests that the SEY reduction effect of the CNTs occurs at energies about an order of magnitude less than simple density arguments predict, perhaps due to the CNT morphology.

Below ~1000 eV the AlSi 129 yield curve is much less than the bare substrate yield curve in Fig. 3(b), as might be expected from a bulk HOPG graphite yield curve (with $\delta_{max} = 1.34$) that is 50% less than that of the AlSi substrate (with $\delta_{max} = 2.02$) at this energy. However, below 500 eV the AlSi 129 yield curve is below both the bare AlSi substrate and the HOPG curve. Again, this suggests that there are substantial additional factors in reducing the CNT forest sample low-energy yields that is attributed to the CNT morphology.

Upon closer inspection in Fig. 4(a), from 1000-5000 eV the SEY yield of the CNT forest samples are actually higher than those of the bare substrate. This can be caused by a reduced attenuation of the electrons backscattered from the substrate due to the lower BSEY of the carbon atoms, thereby generating graphitic secondary electrons adding to the total yield of the samples.

For all of the CNT forests samples, it is interesting to note that the largest yield lies just above unity from ~600-1500 eV, with AlSi 132 reaching the highest value of 1.16 ± 0.02. There are weak trends amongst the CNT forest samples with increasing E_{max}, and decreasing E_1 for the AlSi 127, AlSi 129 and AlSi 132 samples, respectively (see Table II). There is also a weak trend for decreasing δ_{max} with increasing surface density for these three sample (see Table I); such a trend is consistent in order and magnitude with increased yield suppression scaling with the density of C atoms above the substrate. The AlSi 132 yield curve in Fig. 4(b) also has some increased points between 400-700 eV; considering some of the SEM images of the AlSi 132 sample, this might be attributed to defects.

The only significant variance in the SEY amongst the CNT forests samples occurs between energies of 30-100 eV (see Fig. 4(b)). AlSi 129, the tallest and denser sample, has the lowest SEY with values about 10% lower than the AlSi 132 sample in this region. AlSi 132 has a lower density than AlSi 127, but is slightly taller on average. AlSi 132 has a lower yield from 40-150 eV, suggesting the possibility that the forest height could have more of an influence for lowering yield than the relative densities.

The backscatter yield curves for the CNT forest samples agree with each other to within measurement errors (see Fig. 4(c)); they are also of similar magnitude to the HOPG BSEY curves [20]. All the CNT forest sample BSEY curves are ~2.5 times less than those of the bare AlSi substrate over the full energy range. Thus, the CNT forest coatings tend to suppress the BSEY of the substrate, regardless of their density and height. As with the SEY results, this suggests that there are substantial additional factors lowering the CNT forest sample low-energy yields related to the CNT morphology. Note at energies below 30 eV, the larger BSEY yields suggest that there may be some unmitigated charging effects that act to boost SE to energies above 50 eV.

VI. Conclusions

Total, secondary and backscatter electron yield data taken with beam energies between 15 eV and 30 keV demonstrate that carbon nanotube (CNT) forest coatings on substrates substantially suppress substrate yields. At incident electron

energies above ~1200 eV the substrate yields dominated those of the CNT forests, as incident electrons penetrated through the low-density, low-Z CNT forests and backscattered from the higher-Z substrate. Above ~1200 eV, the yield of the forests is slightly higher than the bare substrate, which may result from lower attenuation of SE produced by BSE directed back out of the substrate. This energy is about an order of magnitude lower than density arguments of solid materials would account for. This implies a need for more rigorous mass density measurements of CNT forest samples, but can also suggest that the morphology has a large influence on the scattering of SE and BSE within the forest, enhancing their trapping effect. At lower energies <1200 eV, the CNT forests substantially reduced the overall yields of the substrate, and for <600 eV CNT forest yields were <1 and well below the already low yields of bulk graphite. This increased E_1 up to ~600 eV for the CNT forest samples well above an E_1 of 36 eV of the AlSi substrate, and limited the positive charging regime to between ~600-1600 eV. Although the CNT yield reduction occurs only at energies below ~1200 eV, most materials' E_{max} lie below this energy, and CNT forests are therefore still effective at minimizing δ_{max}. The yield's dependence on the height and density of the CNT forest is a relatively small effect, but is consistent with increased influence of carbon scatter as the density and interaction time with C atoms increases.

References

[1] V. Baglin, J. Bojko, O. Grobner, B. Henrist, N. Hilleret, C. Scheuerlein and M. Taborelli, "The Secondary Electron Yield of Technical Materials and its Variation with Surface Treatments" in *EPAC,* Vienna, Austria, Sep. 2000, rpt. 433.

[2] D. Ruzic, R. Moore, D. Manos, and S. Cohen, "Secondary electron yields of carbon-coated and polished stainless steel," *J. Vacuum Sci. and Tech.*, vol. 20, iss. 4, 1313, 1982.

[3] A. Curren, "Carbon and carbon-coated electrodes for multistage depressed collectors for electron beam devices: a technology review," *IEEE Trans. Electron Devices*, vol. ED-33, no. 11, pp. 1902-1914, 1986.

[4] C. Jin, A. Ottaviano, and Y. Raitses. "Secondary electron emission yield from high aspect ratio carbon velvet surfaces" *J. Appl. Phys.*, vol. 122, iss. 17, 173301, 2017.

[5] M. K. Alam, P. Yaghoobi, M. Chang, A. Nojeh, "Secondary Electron Yield of Multiwalled Carbon Nanotubes" (2010) *Appl. Phys. Lett.*, vol. 97, iss. 26, 2010.

[6] R. Valizadeh, O. B. Malyshev, S. Wang, S. A. Zolotovskaya, W. A. Gillespie, and A. Abdolvand, "Low secondary yield engineered surface for electron cloud mitigation," *Appl. Phys. Lett.,* vol. 105, 231605, 2014.

[7] L. Olano, M. E. Dávila, J. R. Dennison, and I. Montero, "Dynamic secondary electron emission in rough composite materials," submitted to *J. Appl. Phys.,* 2018**.**

[8] J. d. Lara, F. Perez, M. Alfonseca, L. Galan, I. Montero, W. Roman, and D. R. Garcia-Baquero, "Multipactor prediction for on-board spacecraft RF equipment with the MEST software tool," *IEEE Trans. Plasma Sci.,* vol. 34, no. 2, pp. 476-484, 2006.

[9] J. Wilson, E. Wintucky, K. R. Vaden, D. A. Force, I. L. Krainsky, R. N. Simons, N. R. Robbins, W. L. Menninger, D. R. Dibb, and D. E. Lewis, "Advances in space traveling-wave tubes for NASA missions," *Proc. IEEE,* vol. 95, no. 10, 1958-1967, Oct. 2007.

[10] N. Nickles, R. E. Davies and J. R. Dennison, "Applications of Secondary Electron Energy- and Angular-Distributions to Spacecraft Charging," *Proc. 6th Spacecraft Charging Tech. Conf.*, Hanscom Air Force Base, MA, 2000.

[11] G. G. Tibbetts, "Why are carbon filaments tubular?" *J. Crystal Growth*, vol. 66, pp. 632-638, 1983.

[12] B. D. Wood, J. S. Dyer, V. A. Thurgood, N. A. Tomlin, J. H. Lehman, T.-C. Shen, "Optical Reflection and Absorption of Carbon Nanotube Forest Films on Substrates," *J. Appl. Phys.,* vol. 118, iss. 1, 2015.

[13] G.F. Zhong, T. Iwasaki, H. Kawarada, "Semi-quantitative study on the fabrication of densely packed and vertically aligned single-walled carbon nanotubes," *Carbon,* vol. 44, iss. 10, 2009-2014, 2016

[14] J. R. Dennison, J. C. Gillespie, A. Andersen, A. E. Jensen, J. Dekany, G. Wilson, A. M. Sim, and R. Hoffmann, "Synergistic Models of Electron Emission and Transport Measurements of Disordered SiO_2," *Proc.* 14*th Spacecraft Charging Tech. Conf.,* ESA/ESTEC, Noordwijk, NI, 2016.

[15] J. Christensen, "Electron Yield Measurements of High-Yield, Low Conductivity Dielectric Materials," M.S. Thesis, Dept. of Physics, USU, Logan, UT, 2017.

[16] N. Balcon, D. Payan, M. Belhaj, T. Tondu, V. Inguimbert, "Secondary Electron Emission on Space Materials: Evaluation of the Total Secondary Electron Yield from Surface Potential Measurements," *IEEE Trans. Plasma Sci.,* vol. 40, no. 2, 2012.

[17] W. N. Hansen, G. J. Hansen, Standard reference surfaces for work function measurements in air," Surf. Sci. 481, 172-184, 2001.

[18] M. Shiraishi, M. Ata, "Work Function of Carbon Nanotubes," Carbon, vol. 39, iss. 12, 1913-1917, 2001.

[19] G. Wilson, A. Starley, J. R. Dennison "Electron Range Computational Tool for Arbitrary Materials Over a Wide Energy Range," *15th Spacecraft Charging Tech. Conf.,* Kobe, Japan, June 25-29, 2018.

[20] R. C. Hoffmann and J. R. Dennison, "Methods to Determine Total Electron-Induced Electron Yields Over Broad Range of Conductive & Nonconductive Materials," *IEEE Trans. Plasma Sci.*, vol. 40, iss. 2, 298-304, 2011.

[21] J. R. Dennison, "Absolute Electron Emission Calibration: Round Robin Tests of Au and Graphite," 14th Spacecraft Charging Technology Conference, ESA/ESTEC, Noordwijk, NL, 2016.

[22] W.Y. Chang, J.R. Dennison, J. Kite and R.E. Davies, "Effects of Evolving Surface Contamination on Spacecraft Charging," Paper AIAA-2000-0868, *Proc. 38th AIAA Meeting on Aerospace Sci.*, Reno, NV, 2000.

[23] J. Christensen, P. Lundgren, J. R. Dennison, "Parameterization of Secondary and Backscatter Electron Yields for Spacecraft Charging," *15th Spacecraft Charging Tech. Conf.,* Kobe, Japan, June 25-29, 2018.